Uniform electron gas at finite temperatures

Travis Sjostrom[1,*] and James Dufty[2]

[1]*Theoretical Division, Los Alamos National Laboratory, Los Alamos, New Mexico 87545, USA*

[2]*Department of Physics, University of Florida, Gainesville Florida 32611, USA*

(Received 8 August 2013; revised manuscript received 3 September 2013; published 12 September 2013)

We calculate the free energy of the quantum uniform electron gas for temperatures from near 0 to 100 times the Fermi energy, approaching the classical limit. An extension of the Vashista-Singwi theory to finite temperatures and a self-consistent compressibility sum rule is presented. Comparisons are made to other local-field correction methods, as well as recent quantum Monte Carlo simulation and classical map-based results. Accurate fits to the exchange-correlation free energy from both theory and simulation are given for future practical applications.

DOI: 10.1103/PhysRevB.88.115123 PACS number(s): 71.10.Ca, 71.15.Mb

I. INTRODUCTION

The uniform, or homogeneous, electron gas (UEG), also known as jellium or as a one-component plasma, is a well-studied system in physics. It is important as a proving ground for method development. Accurate results provide a better understanding of the rich underlying physics of classical and quantum Coulomb correlations, as well as providing a basis for approximations in more complicated real systems. One important case of note is density functional theory at zero temperature, in which local density approximations (LDAs) using the UEG results for the exchange-correlation (XC) energy have proved remarkably successful in systems as diverse as molecules to exotic phases of highly compressed matter.[1,2] A challenge in current research is simulations of warm dense matter, motivating the pursuit of accurate finite-temperature UEG results for the corresponding development of temperature-dependent functionals.

The zero-temperature UEG was the subject of much theoretical development in the 1960s and 1970s of the last century. Random phase approximation (RPA) and beyond-RPA dielectric approximations were particularly successful[3–6] in appropriate limits. However, in 1980 Ceperley and Alder[7] produced benchmark quantum Monte Carlo (QMC) results with nearly exact accuracy across a wide range of densities, though the fixed-node approximation does lead to small errors in the results for high densities. These accurate values for the UEG XC energy provided the essential LDA needed for designing functionals beyond the LDA.[8] Almost all subsequent zero-temperature density functional theory (DFT) formulations make use of this LDA obtained from the UEG simulation in some explicit way. The corresponding LDA for development of finite-temperature DFT, firmly based in the finite-temperature UEG, has been lacking up until now.

There has been much less development for the finite-temperature UEG, due in part to lack of experimental motivation. Today, experimental conditions of warm dense matter span the range from zero temperature to far above the Fermi temperature. Until very recently[9] there have not been any QMC-type simulations in this range to extend those of Ceperley and Alder at zero temperature. However, there have been QMC investigations into more realistic systems at finite temperature, such as hydrogen.[10–12] For the UEG, RPA calculations were originally done by Gupta and Rajagopal[13] and later revised and fits provided by Perrot and Dharma-wardana.[14] Shortly afterward, beyond-RPA calculations were done including static[15,16] and dynamic[17] local-field corrections (LFCs). A finite-temperature Vashista-Singwi (VS)–type calculation was done using an approximate form for the LFCs.[18] In addition other methods have been proposed including the so-called modified convolution approximation[19] and interpolation approximations.[20] Most recently, methods of mapping the quantum problem to a corresponding classical system have been proposed,[21,22] where effective classical strong coupling methods such as molecular dynamics simulation and liquid state theory can be applied.[23] Further details of some of these theories are given in the results and comparisons sections.

Two thermodynamic parameters are required to describe the equilibrium UEG, chosen here to be the density n and temperature T. When measured relative to the Fermi temperature, the dimensionless temperature is

$$t \equiv k_B T/E_F, \tag{1}$$

where $E_F = \hbar^2 q_F^2/2m_e$ is the Fermi energy, and $q_F = (3\pi^2 n)^{1/3}$ is the Fermi wave vector. The density is typically specified in terms of the electron Wigner-Seitz length $r_0 = (4\pi n/3)^{-1/3}$. When measured relative to the Bohr radius $a_B = \hbar^2/(m_e e^2)$, its dimensionless form is

$$r_s \equiv r_0/a_B. \tag{2}$$

Dimensionless thermodynamic properties therefore can be expressed as functions of t and r_s. The importance of Coulomb coupling is measured by a coupling constant defined as the ratio of the Coulomb energy for a pair at distance r_0 relative to the kinetic energy per particle. In the classical limit the appropriate kinetic energy is $k_B T$ and the classical coupling constant is

$$\Gamma \equiv e^2/(r_0 k_B T). \tag{3}$$

It is related to r_s and t by $\Gamma = 2\lambda^2 r_s/t$, where $\lambda = (4/9\pi)^{1/3}$. At very low temperatures the relevant kinetic energy is E_F and the corresponding coupling constant at $t = 0$ is a function of r_s only.

As previously noted the $t = 0$ limit has seen much development, culminating in high-accuracy *ab initio* simulations. This has also been the case for the classical limit, where the Fermi degeneracy goes to 0, represented by $t \gg 1$.[24] The theoretical development in the intermediate Fermi-degeneracy region mentioned above has not been benchmarked so that the relative accuracy of the various methods is unknown. The objective here is to present an improvement of the finite-temperature VS model by including a consistency requirement

on the dielectric function and the pressure derived from it [the exact compressibility sum rule (CSR) for the small wave-vector limit of the dielectric function]. The temperature dependence of the structure (pair correlation function) and thermodynamics (free energy, compressibility) is calculated from this improved VS approximation (VSa) in the range $0 \leqslant t \leqslant 10$ for a wide range of r_s corresponding to warm dense matter conditions. The approach of the free energy to the classical limit is explored also at much higher temperatures. Comparisons with several other theoretical models and the new QMC simulation results are also given. In this way, some assessment of the quality and trends of the results is established.

II. VASHISTA-SINGWI MODEL WITH SELF-CONSISTENT COMPRESSIBILITY

We calculate the UEG at finite temperature by means of an approximate dielectric function of the form

$$\varepsilon(\mathbf{q},\omega) = 1 - \frac{v_q \chi_0(\mathbf{q},\omega)}{1 + G(\mathbf{q}) v_q \chi_0(\mathbf{q},\omega)}, \tag{4}$$

where $v_q = 4\pi e^2/q^2$ is the Coulomb potential and $\chi_0(\mathbf{q},\omega)$ is the finite-temperature polarizability of the non-interacting UEG, and $G(\mathbf{q})$ is the static LFC. For simplicity of notation, the dependence of these functions on r_s and t is not made explicit except where needed for clarity or emphasis.

The static structure factor is found by the fluctuation-dissipation theorem as a sum over the Matsubara frequencies for the polarizabilities of the interacting system[15] as

$$\begin{aligned} S(\mathbf{q}) &= -(\beta n)^{-1} \sum_{l=\infty}^{\infty} \frac{1}{v_q} \left(\frac{1}{\varepsilon(\mathbf{q},z_l)} - 1 \right) \\ &= -(\beta n)^{-1} \sum_{l=\infty}^{\infty} \frac{\chi_0(\mathbf{q},z_l)}{1 - [1 - G(\mathbf{q})] v_q \chi_0(\mathbf{q},z_l)}, \end{aligned} \tag{5}$$

where $z_l = 2\pi i l/\beta\hbar$ and in the second line we have made the static LFC approximation consistent with Eq. (4).

We choose for $G(\mathbf{q})$ the form given originally by VS[6] in the temperature-dependent generalization

$$\begin{aligned} G(\mathbf{q}) = &\left(1 + a(r_s,t) n \frac{\partial}{\partial n}\right) \\ &\times \left(-\frac{1}{n} \int \frac{d\mathbf{q}'}{(2\pi)^3} \frac{\mathbf{q}\cdot\mathbf{q}'}{q'^2} [S(\mathbf{q}-\mathbf{q}',r_s,t) - 1] \right), \end{aligned} \tag{6}$$

where $a(r_s,t)$ is a parameter determined below. Contained within this form are the LFCs for other finite-temperature calculations. For example, $G = 0$ is the RPA and $a = 0$ is the finite-temperature STLS approximation. In the original introduction by VS, a was taken as a constant equal to $2/3$ for the zero-temperature UEG. This value was chosen to provide better agreement with the CSR (below) for metallic densities, with discrepancies only becoming noticeable around $r_s = 4$.

For a given value of a, Eqs. (5) and (6) form a coupled pair of equations that must be solved self-consistently. The resulting S and G may then be used to calculate the dielectric function and other properties of the UEG. The CSR is an exact property of the UEG given by

$$\lim_{\mathbf{q}\to 0} \varepsilon(\mathbf{q},\omega = 0) = 1 + v_q n^2 \kappa, \tag{7}$$

where κ is the thermodynamic compressibility defined in terms of the pressure by

$$\frac{1}{\kappa} = n \frac{\partial P}{\partial n}. \tag{8}$$

Calculation of the compressibility from an approximate dielectric function will generally result in a value different from that obtained from the derivative of the associated pressure. In order to enforce consistency of the pressure and dielectric forms we define $a(r_s,t)$ for satisfaction at all r_s and t. The two expressions for the compressibility can be written in the equivalent form

$$\frac{\kappa_0}{\kappa} = 1 + \kappa_0 n^2 \frac{\partial^2 (n f_{\rm xc}(n,t))}{\partial n^2} = 1 - \kappa_0 n^2 \gamma 4\pi e^2, \tag{9}$$

where κ_0 is the compressibility for the noninteracting UEG. In the first equality the pressure has been expressed in terms of the XC free energy per particle $f_{\rm xc}$. In the second equality the dielectric function in the form of Eq. (4) has been used, with the definition $\gamma \equiv \lim_{q\to 0} q^{-2} G(q)$.

In order to calculate $f_{\rm xc}$ we perform an integration of the interaction energy over the Coulomb coupling constant. In the following this integration is replaced as an integration over r_s at constant t:[17]

$$f_{\rm xc}(r_s,t) = \frac{1}{r_s^2} \int_0^{r_s} dr_s'\, r_s' e_{\rm int}(r_s',t). \tag{10}$$

Here $e_{\rm int}(r_s,t)$ is the average interaction energy per particle (average Coulomb potential energy), as distinct from the corresponding XC energy. This average interaction energy can be expressed in terms of the structure factor $S(\mathbf{q})$ for evaluation from the above dielectric theories. From this point on, the reduced wave vector $x = q/q_F$ and Hartree atomic units ($\hbar = m_e = e = 1$) are used. The XC free energy per particle is then given by

$$f_{\rm xc}(r_s,t) = \frac{1}{\pi\lambda r_s^2} \int_0^{r_s} dr_s' \int_0^{\infty} dx\, [S(x) - 1]. \tag{11}$$

For numerical evaluation Eqs. (5) and (6) are written in the forms

$$S(x) = \frac{3}{2} t \sum_{l=-\infty}^{\infty} \frac{\Phi(x,l)}{1 + (2\Gamma t/\pi\lambda x^2)[1 - G(x)]\Phi(x,l)}, \tag{12}$$

where

$$\begin{aligned} \Phi(x,l) &= -\frac{\pi^2}{q_F} \chi_0(q,z_l) \\ &= \frac{1}{2x} \int_0^{\infty} \frac{dy\, y}{e^{y^2/t - \eta} + 1} \ln \left| \frac{(2\pi l t)^2 + (x^2 + 2xy)^2}{(2\pi l t)^2 + (x^2 - 2xy)^2} \right| \end{aligned} \tag{13}$$

is the dimensionless free-electron polarizability. Here $\eta = \beta\mu_0$, where μ_0 is the chemical potential of the noninteracting system, which may be found from t through the Fermi integral

$$I_{1/2}(\eta) = \frac{2}{3} t^{-3/2}. \tag{14}$$

Additionally, we make use of the equivalent expression for $S(x)$ given in Ref. 15 [their Eq. (27)], which allows for efficient computation in the short-wavelength regime.

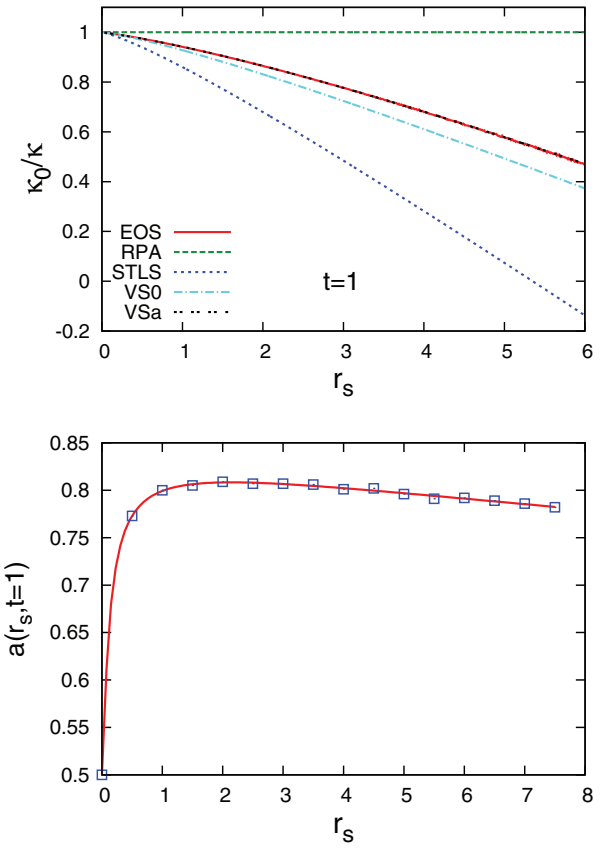

FIG. 1. (Color online) Top: Compressibility ratio from the sum rule is plotted for various approximate dielectric functions, along with the ratio from the equation of state. Bottom: The self-consistent $a(r_s,t)$ which satisfies the CSR at $t = 1$.

Equation (6) is then given by

$$G(x) = G_I(x) + a(r_s,t)\left(-\frac{x}{3}\frac{\partial}{\partial x} - \frac{r_s}{3}\frac{\partial}{\partial r_s}\right) G_I(x), \qquad (15)$$

where

$$G_I(x) = -\frac{3}{4}\int_0^\infty y^2\,[S(y) - 1]\left(1 + \frac{x^2 - y^2}{2xy}\ln\left|\frac{x+y}{x-y}\right|\right) dy.$$

In practice, the derivatives with respect to x and r_s are taken by finite-difference approximations. For x this is simply done for a calculation at any r_s and t. However, for r_s this requires having $G(x)$ for neighboring r_s so we solve self-consistently five points simultaneously $[r_s - 2\delta, r_s - \delta, r_s, r_s + \delta, r_s + 2\delta]$. The derivative and second derivative of the central point are solved using finite differences, and the derivatives of the neighboring points are given by Taylor expansion about the central point using its second derivative.

Beyond the self-consistency for S and G we impose self-consistency of Eqs. (9) and (11) to find $a(r_s,t)$. Figure 1 shows the results for $t = 1$ as a function of r_s. The top panel shows the compressibility ratio calculated from the equation of state (EOS) [first equality of Eq. (9)] in comparison with that calculated from the dielectric function [second equality of Eq. (9)]. Several choices for G are illustrated: RPA ($G = 0$), STLS ($a = 0$), the $t = 0$ VS0 ($a = 2/3$), and the CSR constrained result here, the VSa [$a(r_s,t)$]. All of the methods produce nearly identical results for the EOS calculations and are shown by the single curve labeled EOS. Clearly the only results that satisfy the CSR is our curve where it is enforced. The lower panel shows the self-consistent value of $a(r_s,t = 1)$ as a function of r_s. Qualitatively similar results are obtained at other temperatures as well.

We perform the self-consistent calculation for $a(r_s,t)$ over the temperature and density plane at the values $t = [0.0625,0.125,0.25,0.5,1.0,1.5,2,3,4,6,8,10]$ and r_s at integer and half-integer values from 0 to 10. For r_s, however, the self-consistent calculation requires a fit of $a(r_s,t)$ for all r_s and so those calculations for a given t are performed for r_s at 0.01 spacing from 0 to 10. Integration for $S(x)$ and $G(x)$ are done up to $x = 240$, and the Matsubara frequencies are summed up to $|l| = 1000$.

III. RESULTS AND COMPARISONS

Before presenting the results of our calculations we provide a brief list of other methods and note those used for comparisons here. First, we consider the dielectric models described above, the RPA, STLS, and VSa (present work). The above method for calculation is applied to all three, and it is confirmed that the RPA and STLS results are in agreement with those provided in the original studies.[13–15] The STLS was extended to include dynamic LFCs in the "quantum" STLS (QSTLS) method,[17] though the QSTLS shows negligible energy differences from the STLS for $t > 1$. The modified convolution approximation makes use of a static LFC but solves a different set of integral equations for S and G.[19] Interpolative Padé fits for high density, low density, and classical limits are given by Ebeling[20] and Kremp *et al.*[25] A quite different approach attempts to apply classical strong-coupling methods to the UEG using a quantum modified Coulomb potential and effective thermodynamic parameters. The classical-map hypernetted-chain method (CHNC) maps a quantum system with temperature T to a classical system with temperature T_{cf} for which classical calculations of correlation energy, pair distribution functions, etc., are taken for the quantum system.[21] Another classical map enforces the equivalence of the grand potential and two of its derivatives between a quantum and a classical system.[22] Finally, restricted path integral Monte Carlo (RPIMC) simulation results have been performed over the temperature and density range of interest.[9] The presentation below compares our VSa results with other dielectric models (RPA, STLS), classical map (CHNC), and quantum simulations (RPIMC). Also shown for reference are the classical Monte Carlo (CMC) simulations.[24]

A. Interaction energy

Two equivalent expressions for the XC free energy are given in Eqs. (10) and (11) as integrations over the coupling constant (converted to r_s) of the interaction energy or structure factor, respectively. The latter is convenient for evaluation of the theories above, but the former is useful for analysis of the results provided by RPIMC. In the RPIMC the primary results are the total average kinetic k and average potential energies v, which give the total internal energy $e_{\rm tot} = k + v$ (lowercase letters indicate per particle). v is in fact the interaction energy $e_{\rm int}$ that appears in Eq. (10). This is different from the XC energy,

e_{xc}, whose RPIMC values are the basis for the numerical fit which is provided in Ref. 9: $e_{xc} = e_{tot} - e_0$, where $e_0 = k_0$ is the ideal-gas kinetic energy. The XC energy is related to the XC free energy by the thermodynamic identity $e_{xc} = f_{xc} + Ts_{xc}$, where s_{xc} is the excess entropy. Here we prefer to work with $e_{int}(r_s,t)$, also provided in the RPIMC results.[9]

To facilitate the comparison of theory and simulation, we first fit the RPIMC interaction energy data (see Appendix). The corresponding $e_{int}(r_s,t)$ from theory is obtained by a comparison of Eqs. (10) and (11) for the identification

$$e_{int}(r_s,t) = \frac{1}{\pi\lambda r_s}\int_0^\infty dx\ [S(x)-1]\,|_{t,r_s}. \tag{16}$$

The numerical fit using STLS has been given in Ref. 29; the corresponding fit using VSa is given here (Appendix). Next, these fits are used in Eq. (10) to obtain the XC free energy f_{xc} for RPIMC, STLS, and VSa. Existing fits for f_{xc} from CHNC and CMC are also considered in the following.

We stress the importance of fits for f_{xc} value for finite-temperature DFT and other applications, rather than those for e_{xc}. It is the former that is required for the finite-temperature LDA in the construction of XC functionals. The remainder of this paper continues analysis of the various methods for cross validation and assessment of the best approximation to be used.

The interaction energy per particle divided by the temperature is directly compared in Fig. 2 for the RPIMC, VSa, and STLS at $t = 1$. The uncertainties for the interaction energy

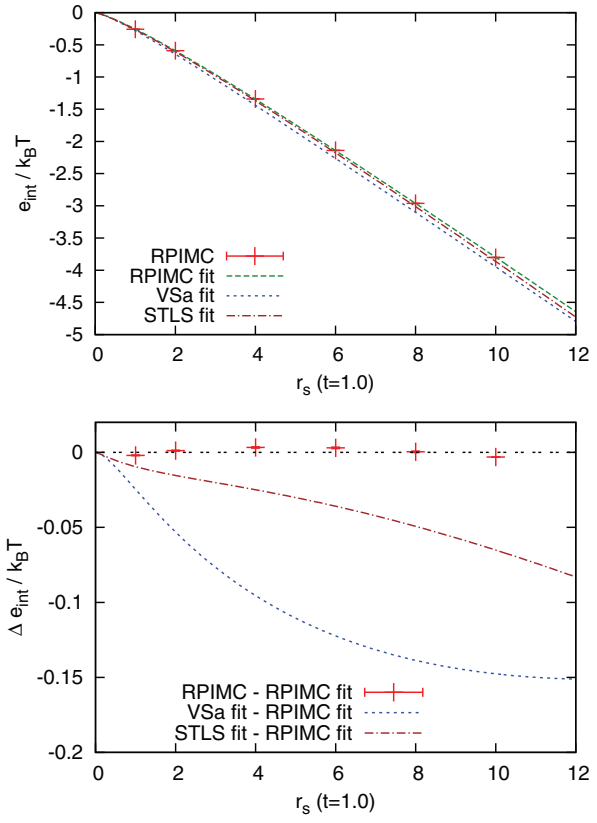

FIG. 2. (Color online) Interaction energy from RPIMC data and fits for RPIMC, VSa, and STLS as given in the Appendix. The bottom panel shows differences of RPIMC data and VSa and STLS fits compared with the RPIMC fit.

as quoted in Ref. 9 are shown but not visually discernible in these plots. The trends seen here hold for all t: the fit for the RPIMC is a very accurate representation of the raw data; the finite-temperature STLS is a very good approximation to the RPIMC, while its "improved" version, the VSa, is also good but with a larger discrepancy from the RPIMC. All subsequent figures utilize the RPIMC fit in lieu of the limited RPIMC data.

B. Equation of state

The free energy is defined here as the sum of the noninteracting free energy and the XC free energy $F = F_0 + F_{xc}$, where we consider the free energy per particle $F/N = f$. The noninteracting free energy per particle is given by

$$f_0 = F_0/N = -\frac{2}{3\beta}\frac{I_{3/2}(\eta)}{I_{1/2}(\eta)} + \frac{\eta}{\beta}. \tag{17}$$

The XC free energy per particle, f_{xc}, for this work is given by Eq. (11). Similarly, the pressure is $P = P_0 + P_{xc}$ and found from the derivative of the free energy per particle for the components, $P = n^2\, d(n(f_0 + f_{xc}))/dn$. Additionally, one may separate f_{xc} into exchange only (X) and correlation (C) components using the known value for f_x,

$$f_x = -\frac{1}{2\pi}\left(\frac{\beta}{2}\right)^{1/2}\frac{\int_{-\infty}^{\eta}[I_{1/2}(x)]^2\,dx}{I_{1/2}(\eta)}, \tag{18}$$

leaving the correlation component as the only value to calculate. However, direct evaluation of Eq. (11) provides the XC contribution as a single term and fits are usually given for XC, so we plot in Fig. 3 the XC free energy per particle, f_{xc}, relative to the XC energy at zero temperature (known from zero-temperature QMC calculations). The classical, high-temperature Debye-Hückel (DH) limit has no exchange contribution and the correlation component to first order is $f_c = -\frac{1}{3}\lambda_D + \cdots$, with $\lambda_D = (4\pi n\beta)^{1/2}$. However, encompassing this limit are the CMC results of Hansen,[24] which are shown (Ref. 24 also provides quantum corrections, but only the classical excess free energy is shown here).

In Fig. 3, we note first that there is a significant temperature dependence predicted by all models for both $r_s = 1$ and $r_s = 4$ over the whole range considered, $0 \leqslant t \leqslant 10$. Our VSa results lie between those for the RPA (not shown) and the STLS. This trend holds true for other properties, such as $G(q)$, $S(q)$, and $g(r)$, as well. The CHNC (using the fit provided in Ref. 21) is systematically below these; like the STLS it is a better approximation to the RPIMC than the VSa, although all are quite similar. All of the methods appear to be approaching the classical limit in the same manner. The outlier is the Padé interpolation, due in large part to the low-t limit being constructed to go to the Gell-Mann Brueckner limit as opposed to the exact limit for larger r_s.

C. Pair correlation function

The pair correlation function $g(r)$ is calculated from the static structure factor by

$$g(r) = 1 + \frac{3}{2r}\int_0^\infty x\sin(xr)[S(x)-1]dx, \tag{19}$$

where r is in units of q_F^{-1}.

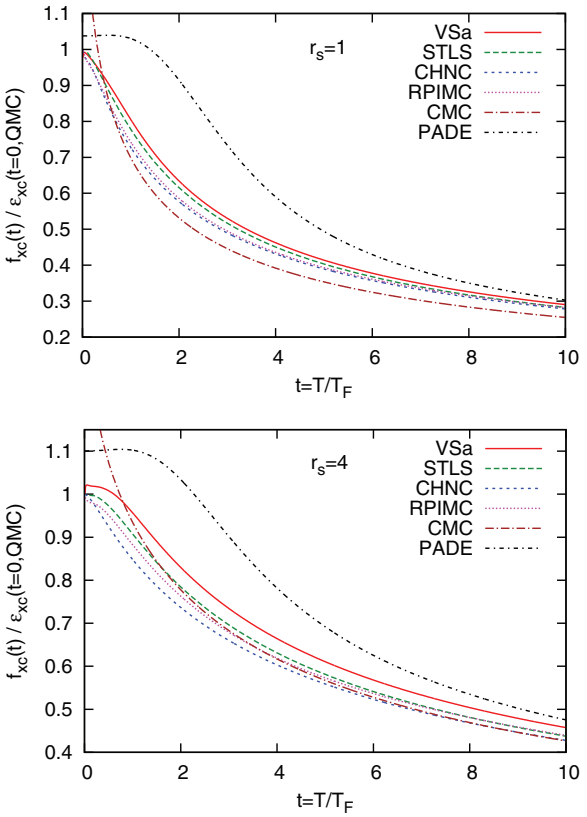

FIG. 3. (Color online) XC free energy for several calculations, with the classical limit plotted for comparison, relative to the known zero-temperature XC energy.

The approximate dielectric methods are compared with the RPIMC and the classical map of the Perrot and Dharmawardana CHNC in Fig. 4. Another classical map,[22] (not shown in figure) also gives results close to those of RPIMC, and both classical maps have the advantage of preserving the positivity of $g(r)$. Again, there is a significant t dependence between $t = 1$ and 8 in the range $r < 1$ for both $r_s = 1$ and 4. The dielectric methods all have non-physical negative values at short distances for larger r_s as can be seen in the $r_s = 4$ panels. STLS is least negative, though the VSa is much closer to the STLS than it is to the RPA.

D. Compressibility

Our VSa, by construction, is the only approximate dielectric function considered here that satisfies the CSR; the STLS, for example, does not. For comparison of the VSa with the nondielectric methods we consider the compressibility as calculated from the EOS as given in Eq. (9) for all methods. We evaluate the required derivatives for the compressibility from the f_{xc} fits mentioned above. The CHNC is not shown, as the f_{xc} fit has some irregularity, which shows up in the derivatives as occasional wiggles in the compressibility ratio. We note that those fits were constructed for the free energy, not the compressibility.

In Fig. 5 the compressibility ratio κ_0/κ is plotted at several values of t as a function of r_s. A first surprising observation is that the purely classical simulation (CMC) provides

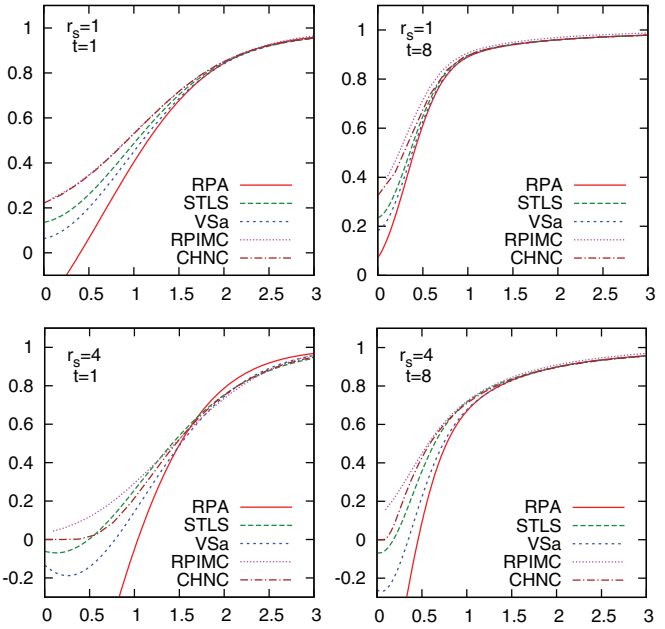

FIG. 4. (Color online) Pair correlation functions at given t and r_s. The y and x axes represent $g(r)$ and r (in units of q_F^{-1}), respectively.

semiquantitative agreement with the quantum theories and simulations, except at the smallest t shown. At the lowest temperature all of the quantum methods are close to the original VS $T = 0$ results, crossing 0 just above $r_s = 5$. As with the f_{xc} shown in Fig. 3, the STLS results lie in between the VSa and the RPIMC results. At the highest temperature these three results are essentially indistinguishable.

An interesting feature of the UEG is that at all temperatures there is a maximum r_s beyond which the compressibility becomes negative. This apparent instability of the UEG system is not necessarily a true thermodynamic instability, however,

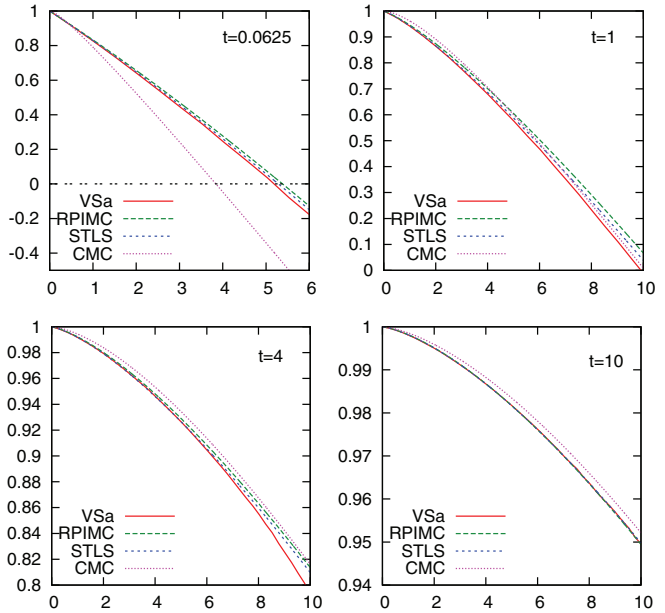

FIG. 5. (Color online) Compressibility ratio κ_0/κ (y axis) as a function of r_s (x axis) for a given t.

TABLE I. Values of r_s for which the compressibility becomes negative for several t. Also shown are the Coulomb coupling constant and Debye-Hückel parameter evaluated at the VSa r_s.

t	VSa	STLS	RPIMC	CMC	Γ	λ_D
0.0625	5.23	5.29	5.38	3.85	45.4	2.23
1	9.88	10.3	10.6	10.1	5.36	0.406
4	33.2	35.0	35.2	34.4	4.51	0.111
10	82.8	86.0	85.4	84.5	4.49	0.044

as we have assumed a uniform background which adjusts to neutralize the system at no energy cost.[26,27] At zero temperature this maximum is just above $r_s = 5$. For the case of real metals, which of course are not true UEGs, Cs has the largest value, at $r_s = 5.63$.[28] This instability is far above the density for the onset of Wigner crystallization. Also known at zero temperature is a crossover to a spin-polarized system before Wigner crystallization and, also, the possible existence of more exotic states such as charge density wave and spin density wave.[26,27] Here we only examine the non-spin-polarized UEG system and the onset of negative compressibility in such a state. In Table I we record this maximum r_s as given by the VSa, STLS, RPIMC, and CMC (which includes classical strong-coupling contributions beyond DH).[24] Also listed are the Coulomb coupling constant, $\Gamma = 0.543\, r_s/t$, and the DH parameter, $\lambda_D = 1.276/\sqrt{t r_s}$, both evaluated at the value of r_s for the instability predicted from the VSa.

E. Classical limit

The ideal Fermi gas thermodynamics depends on n and T only through t, and at $t = 10$ the classical limit is approached. For the interacting UEG, properties depend on both t and r_s through the Coulomb interactions and the large-t classical limit is not uniform in r_s. For a fixed r_s there is a sufficiently large t above which the classical limit applies. However, within this limit the DH limit need not apply. The latter requires, in addition, a small Γ. In order to examine the classical limit we consider the case $r_s = 1$ in the large-t limit. In this limit correct results should come into agreement with the DH result since Γ is small, and the fits are mostly constructed to do so. Figure 6 shows the XC free energy for $r_s = 1$ and t from 10 to 100. In the top panel the XC free energy shows agreement among all of the quantum methods: the VSa, STLS, RPIMC, and CHNC. Additionally, the classical DH and CMC are in very good agreement with each other, with small differences becoming visible below $t = 25$. The difference between these classical results and the quantum results is mainly due to the exchange contribution, f_x, which is shown near the top of the plot. In the bottom panel, to highlight the differences of the quantum methods, $f_{\rm xc}$ is multiplied by $t^{1/2}$, since the DH limit is proportional to $t^{-1/2}$ for a fixed r_s. In addition, the classical methods are shown with f_x added.

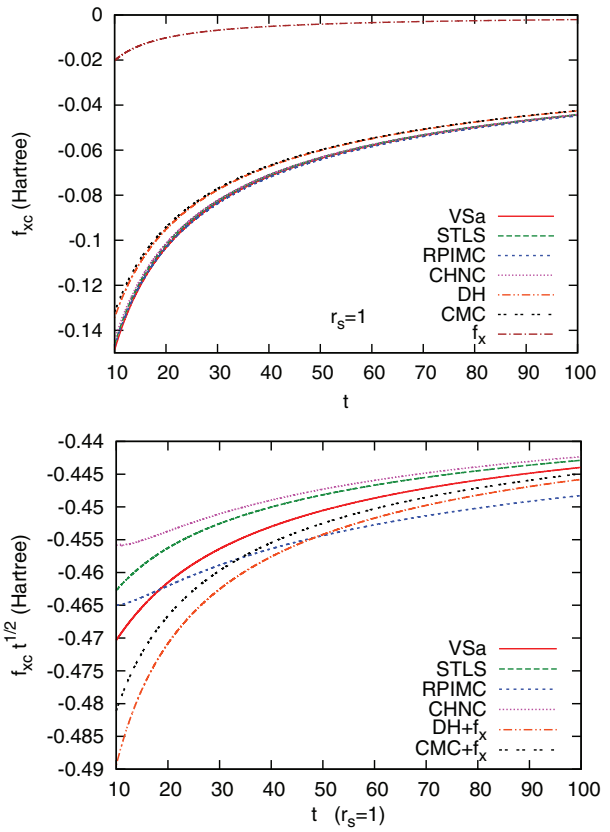

FIG. 6. (Color online) Comparison of XC free energies for large t at $r_s = 1$. In the bottom plot the exchange free energy f_x has been added to the classical results.

IV. CONCLUSIONS

In this work we have presented calculations for the UEG from an approximate dielectric function method based on a finite-temperature version of the VS static LFC, modified to enforce the CSR at all t and r_s. This sum rule is violated by the original $t = 0$ VS(0) and by previous finite-temperature RPAs and STLS approximations.

We have made comparisons of equilibrium structure and thermodynamics calculations with other finite-temperature RPA, STLS, and classical mapping methods and with RPIMC results. Our VSa method in general produces results between those for the RPA and the STLS, though closer to the STLS, for the UEG properties considered: $G(k)$, $S(k)$, $g(r)$, $f_{\rm xc}$, and κ. For $f_{\rm xc}$, dielectric methods and classical map methods are similar, as is our fit for the RPIMC. The results for the compressibility follow these same trends. This includes some deviation of the VSa from the STLS and RPIMC methods for intermediate r_s, and t values. For $g(r)$ the dielectric methods produce unphysical negative values at small r and large r_s, with the VSa slightly more negative than the STLS, while both the RPIMC and classical map methods produce non-negative $g(r)$. The simplest dielectric approach, RPA, is not shown here [except for the $g(r)$ results], as the deviation from other methods is generally quite large.

Perhaps surprisingly, the VSa with internal consistency for the CSR deviates somewhat more from the RPIMC results than its underlying STLS method without this consistency. We believe the reason for this can be seen in Fig. 1. There, in order for the CSR to be satisfied, the STLS curve must shift up towards the RPA curve, the result being a more RPA-like result. The results then demonstrate a lack of flexibility of the VS/VSa static local-field model in that, while correcting for the CSR,

the resulting f_{xc} energies and $g(r)$ accuracy are diminished, results that are consistent with the original zero-temperature STLS and VS results.

Finally, we see that the STLS and RPIMC in fact cross-validate each other very nicely. It has long been known that STLS gives quite good zero-temperature XC energies compared to QMC results, and this seems to be true for finite temperatures as well. This good agreement is also seen to apply for the interaction energy (e.g., Fig. 2). This contrasts somewhat with the comparisons of XC energy and RPIMC in the recent fit analysis by Brown *et al.*[9] One must also consider the RPIMC data, which show increasing error for smaller r_s and are currently uncorroborated by other QMC-type results.

In summary, we have compared the most accurate approximations of f_{xc} and found them to be close, but in particular, the STLS and RPIMC seem to pin down the correct results. This lends theoretical support for the simulations and their extension by the fit for the RPIMC f_{xc} given here. An important application, to be discussed further elsewhere, is the implementation as a local density functional and the construction of more complex functionals needed for finite-temperature DFT.

ACKNOWLEDGMENTS

The authors thank S. Dutta for providing CHNC calculations of the pair correlation function. This research was supported by US DOE Grant DE-SC0002139. T.S. acknowledges support by the NNSA of US DOE at Los Alamos National Laboratory under Contract No. DE-AC52-06NA25396.

APPENDIX: FITS FOR THE EXCHANGE-CORRELATION FREE ENERGY

An effective fitting procedure for STLS calculations has been given by Ichimaru in Ref. 29 (p. 290); that fit has been used for all STLS plots above. We extend that method in this Appendix to the VSa calculations and RPIMC results. First, the same functional form is chosen for the interaction energy, expressed in terms of Γ,t instead of r_s,t, and a least-squares fitting for the parameters is performed. With the coefficients known and dependence on Γ displayed explicitly, the coupling constant integration of Eq. (10) can be performed to get the XC free energy per particle, f_{xc}.

The interaction energy per particle is given in Hartree units by

$$e_{\rm int}(r_s,t) = -\frac{\Gamma}{\beta}\frac{a(t)+b(t)\sqrt{\Gamma}+c(t)\Gamma}{1+d(t)\sqrt{\Gamma}+e(t)\Gamma}. \tag{A1}$$

Here $a(t)$ is given by the exchange parametrization given in Ref. 14 as

$$a(t) = 0.610887\tanh\left(\frac{1}{t}\right) \times \frac{0.75+3.04363t^2-0.09227t^3+1.7035t^4}{1+8.31051t^2+5.1105t^4}. \tag{A2}$$

TABLE II. Fit parameters for the exchange-correlation free energy for the STLS, VSa, and RPIMC given by Eqs. (A1)–(A7). STLS parameters as given in Ref. 29.

	STLS	VSa	RPIMC
x_1	3.4130800×10^{-1}	1.8871493×10^{-1}	3.4130800×10^{-1}
x_2	1.2070873×10^{1}	1.0684788×10^{1}	8.7719094×10^{1}
x_3	1.148889×10^{0}	1.1088191×10^{2}	4.4699486×10^{3}
x_4	1.0495346×10^{1}	1.8015380×10^{1}	3.4072692×10^{2}
x_5	1.326623×10^{0}	1.2803540×10^{2}	5.1614521×10^{3}
x_6	8.72496×10^{-1}	8.3331352×10^{-1}	8.6415253×10^{-1}
x_7	2.5248×10^{-2}	-1.1179213×10^{-1}	-9.2236194×10^{-2}
x_8	6.14925×10^{-1}	6.1492503×10^{-1}	6.1492503×10^{-1}
x_9	1.6996055×10^{1}	1.6428929×10^{1}	2.5191969×10^{1}
x_{10}	1.489056×10^{0}	2.5963096×10^{1}	1.8208366×10^{1}
x_{11}	1.010935×10^{1}	1.0905162×10^{1}	1.8659964×10^{1}
x_{12}	1.22184×10^{0}	2.9942171×10^{1}	1.8463421×10^{1}
x_{13}	5.39409×10^{-1}	5.3940898×10^{-1}	5.3940898×10^{-1}
x_{14}	2.522206×10^{0}	5.8869626×10^{4}	2.9390225×10^{2}
x_{15}	1.78484×10^{-1}	3.1165052×10^{3}	1.1501733×10^{1}
x_{16}	2.555501×10^{0}	3.8887108×10^{4}	3.2847098×10^{2}
x_{17}	1.46319×10^{-1}	2.1774472×10^{3}	8.7963510×10^{0}

Terms b–e are given by

$$b(t) = \sqrt{t}\tanh\left(\frac{1}{\sqrt{t}}\right)\frac{x_1+x_2t^2+x_3t^4}{1+x_4t^2+x_5t^4}, \tag{A3}$$

$$c(t) = \left[x_6+x_7\exp\left(-\frac{1}{t}\right)\right]e(t), \tag{A4}$$

$$d(t) = \sqrt{t}\tanh\left(\frac{1}{\sqrt{t}}\right)\frac{x_8+x_9t^2+x_{10}t^4}{1+x_{11}t^2+x_{12}t^4}, \tag{A5}$$

$$e(t) = t\tanh\left(\frac{1}{t}\right)\frac{x_{13}+x_{14}t^2+x_{15}t^4}{1+x_{16}t^2+x_{17}t^4}. \tag{A6}$$

The fit parameters are chosen to give the correct high-t limit. In Table II we provide our new fit parameters for both the VSa and the RPIMC, as well as those for the STLS from Ref. 29. The coupling constant integration to give the XC free energy is also given in Ref. 29 as

$$\begin{aligned} f_{xc}(r_s,t) = &-\frac{c}{e}\frac{\Gamma}{\beta}-\frac{2}{e}\left(b-\frac{cd}{e}\right)\frac{\sqrt{\Gamma}}{\beta}-\frac{1}{\beta e}\left[\left(a-\frac{c}{e}\right)\right.\\ &\left.-\frac{d}{e}\left(b-\frac{cd}{e}\right)\right]\ln\left|e\Gamma+d\sqrt{\Gamma}+1\right|\\ &+\frac{2}{\beta e\sqrt{4e-d^2}}\left[d\left(a-\frac{c}{e}\right)\right.\\ &\left.+\left(2-\frac{d^2}{e}\right)\left(b-\frac{cd}{e}\right)\right]\\ &\times\left[\tan^{-1}\left(\frac{2e\sqrt{\Gamma}+d}{\sqrt{4e-d^2}}\right)-\tan^{-1}\left(\frac{d}{4e-d^2}\right)\right]. \end{aligned} \tag{A7}$$

*sjostrom@lanl.gov

[1] B. G. Johnson, P. M. W. Gill, and J. A. Pople, J. Chem. Phys. **98**, 5612 (1993).
[2] P. Haas, F. Tran, and P. Blaha, Phys. Rev. B **79**, 085104 (2009).
[3] J. Lindhard, K. Dan. Vidensk. Selsk. Mat. Fys. Medd. **28**, 8 (1954).
[4] M. Gell-Mann and K. A. Brueckner, Phys. Rev. **106**, 364 (1957).
[5] K. S. Singwi, M. P. Tosi, R. H. Land, and A. Sjölander, Phys. Rev. **176**, 589 (1968).
[6] P. Vashista and K. S. Singwi, Phys. Rev. B **6**, 875 (1972).
[7] D. M. Ceperley and B. J. Alder, Phys. Rev. Lett. **45**, 566 (1980).
[8] J. P. Perdew and A. Zunger, Phys. Rev. B **23**, 5048 (1981).
[9] E. W. Brown, B. K. Clark, J. L. DuBois, and D. M. Ceperley, Phys. Rev. Lett. **110**, 146405 (2013); Data fit is given by E. W. Brown, J. L. DuBois, M. Holzmann, and D. M. Ceperley, Phys. Rev. B **88**, 081102(R) (2013).
[10] K. P. Driver and B. Militzer, Phys. Rev. Lett. **108**, 115502 (2012).
[11] V. S. Filinov, M. Bonitz, W. Ebeling, and V. E. Fortov, Plasma Phys. Controlled Fusion **43**, 743 (2001).
[12] S. A. Trigger, W. Ebeling, V. S. Filinov, V. E. Fortov, and M. Bonitz, JETP **96**, 465 (2003).
[13] U. Gupta and A. K. Rajagopal, Phys. Rev. A **22**, 2792 (1980).
[14] F. Perrot and M. W. C. Dharma-wardana, Phys. Rev. A **30**, 2619 (1984).
[15] S. Tanaka and S. Ichimaru, J. Phys. Soc. Jpn. **55**, 2278 (1986).
[16] R. G. Dandrea, N. W. Ashcroft, and A. E. Carlsson, Phys. Rev. B **34**, 2097 (1986).
[17] H. K. Schweng and H. M. Böhm, Phys. Rev. B **48**, 2037 (1993).
[18] W. Stolzmann and M. Rösler, Contrib. Plasma Phys. **41**, 203 (2001).
[19] S. Tanaka and S. Ichimaru, Phys. Rev. B **39**, 1036 (1989).
[20] W. Ebeling, Contrib. Plasma Phys. **30**, 553 (1990).
[21] F. Perrot and M. W. C. Dharma-wardana, Phys. Rev. B **62**, 16536 (2000).
[22] S. Dutta and J. Dufty, Phys. Rev. E **87**, 032102 (2013); Eur. Phys. Lett. **102**, 67005 (2013).
[23] J.-P. Hansen and I. MacDonald, *Theory of Simple Liquids* (Academic Press, London, 2006).
[24] J. P. Hansen, Phys. Rev. A **8**, 3096 (1973).
[25] D. Kremp, M. Schlanges, and W. Kraeft, *Quantum Statistics of Nonideal Plasmas* (Springer-Verlag, Berlin, 2005), p. 256.
[26] G. F. Giuliani and G. Vignale, *Quantum Theory of the Electron Liquid* (Cambridge University Press, Cambridge, 2005), pp. 45–63.
[27] S. Ichimaru, Rev. Mod. Phys. **54**, 1017 (1982).
[28] G. D. Mahan, *Many Particle Physics*, 2nd ed. (Plenum Press, New York, 1990), p. 467.
[29] S. Ichimaru, Rev. Mod. Phys. **65**, 255 (1993).